nature COMMUNICATIONS

ARTICLE

Received 2 Sep 2013 | Accepted 16 Dec 2013 | Published 20 Jan 2014

DOI: 10.1038/ncomms4113

Planar hexagonal B_{36} as a potential basis for extended single-atom layer boron sheets

Zachary A. Piazza[1], Han-Shi Hu[2], Wei-Li Li[1], Ya-Fan Zhao[2], Jun Li[2] & Lai-Sheng Wang[1]

Boron is carbon's neighbour in the periodic table and has similar valence orbitals. However, boron cannot form graphene-like structures with a honeycomb hexagonal framework because of its electron deficiency. Computational studies suggest that extended boron sheets with partially filled hexagonal holes are stable; however, there has been no experimental evidence for such atom-thin boron nanostructures. Here, we show experimentally and theoretically that B_{36} is a highly stable quasiplanar boron cluster with a central hexagonal hole, providing the first experimental evidence that single-atom layer boron sheets with hexagonal vacancies are potentially viable. Photoelectron spectroscopy of B_{36}^- reveals a relatively simple spectrum, suggesting a symmetric cluster. Global minimum searches for B_{36}^- lead to a quasiplanar structure with a central hexagonal hole. Neutral B_{36} is the smallest boron cluster to have sixfold symmetry and a perfect hexagonal vacancy, and it can be viewed as a potential basis for extended two-dimensional boron sheets.

[1] Department of Chemistry, Brown University, Providence, Rhode Island 02912, USA. [2] Department of Chemistry, Key Laboratory of Organic Optoelectronics and Molecular Engineering of Ministry of Education, Tsinghua University, Beijing 100084, China. Correspondence and requests for materials should be addressed to J.L. (email: junli@tsinghua.edu.cn) or to L.-S.W. (email: lai-sheng_wang@brown.edu).

Soon after the discovery of carbon nanotubes[1], analogous boron nanotubes were proposed[2,3]. However, a perfectly planar triangular lattice made of the boron nanotubes is unstable and instead adopts a rather buckled form[4–7]. Recent computational studies suggest that a triangular planar boron lattice with hexagonal vacancies is more stable[8,9], which would be suitable to form the putative boron nanotubes and it underlies the stability of the proposed B_{80} fullerene[10]. However, there has been no experimental evidence for the viability of this newly proposed planar boron sheet. Joint experimental and computational studies over the past decade have shown that boron clusters are planar or quasiplanar at large sizes[11–21], in contrast to bulk boron where three-dimensional (3D) cages are prevalent. Boron clusters with a triangular lattice have invariably found to exhibit out-of-plane distortions[12–17,19–21]. Tetragonal or pentagonal defects are often found in truly planar boron clusters up to 23 atoms[12,17–20].

Here we report the discovery of a quasiplanar boron cluster with sixfold symmetry and a perfect central hexagonal hole, providing the first experimental evidence that large-scale planar boron sheets with hexagonal vacancies are potentially viable. This joint photoelectron spectroscopy (PES) and theoretical study shows that the B_{36}^- cluster is quasiplanar with a central hexagonal hole. Neutral B_{36} is found to be a highly stable cluster with perfect C_{6v} hexagonal symmetry. Extension of this cluster would give rise to the planar boron sheets with hexagonal vacancies[8,9,22,23].

Results

PES of the B_{36}^- cluster. Boron cluster anions with up to 24 atoms have been investigated previously[11–13,16–21]. The PES spectra became more congested and complicated for clusters larger than 20 atoms[19–21], presenting considerable challenges for both computational global minimum searches and comparison between experiment and theory. However, we found that the spectrum of B_{36}^- (Fig. 1a) is special, showing an unusually low electron-binding energy and well-resolved spectral features in the low binding energy side. We also measured the spectrum at 266 nm (not shown) with slightly higher resolution. The adiabatic detachment energy of 3.12 eV measured from the sharp onset of the first detachment band X in the 266 nm spectrum also represents the electron affinity (EA) of neutral B_{36}. It is surprising that the EA of B_{36} is even smaller than that of B_{22} (3.34 eV) (ref. 20) or B_{24} (3.55 eV) (ref. 21), since the EA generally increases with increasing cluster size. The low EA of B_{36} is a result of the large energy gap, as revealed by the X–A separation, suggesting that neutral B_{36} is a highly stable cluster with a large energy gap between its highest occupied (HOMO) and lowest unoccupied (LUMO) molecular orbitals. The weak feature X′ observed in Fig. 1a is due to contributions of a low-lying isomer (*vide infra*). The vertical detachment energies (VDEs) of the observed detachment transitions are given in Supplementary Table 1.

VDEs are usually measured from the peak maxima from PES spectra. For small clusters or simpler systems, PES bands are well separated and each band represents a single detachment transition. In the current case, bands X and A are well resolved and they should each correspond to a single electron detachment channel, as given in Supplementary Table 1. The VDEs for bands X (3.3. eV) and A (4.08 eV) are directly obtained from the band maximum in each case. Band B is relatively broad, which is likely a result of several overlapping detachment transitions. Consequently, a range of energy (4.2–4.5 eV) is given for band B in Supplementary Table 1. Following an energy gap, more congested detachment features are observed above 5 eV, suggesting a high density of electronic states. The label C is given to represent the signals from about 5.1–5.4 eV. An intense band D is observed at ~5.6 eV, which is also likely a result of overlapping detachment transitions. The sharp spikes on the higher binding energy side of band D cannot be assigned as individual detachment transitions because of the relatively low signal-to-noise ratios in this part of the spectrum. Finally, the label E represents the broad signals around 6.1 eV. Hence, all the labels from B to E do not represent individual detachment transitions and they are solely for the sake of discussion. The congested detachment transitions for such a large cluster are expected, as borne out from comparisons with the theoretical results (*infra vide*). The broad X band suggests a significant structural change from the anion to the neutral ground state. Despite the congested spectral features in the higher binding energy side, the relatively simple spectral pattern in the low binding energy side and the large HOMO–LUMO gap indicate that neutral B_{36} should be a highly symmetric cluster.

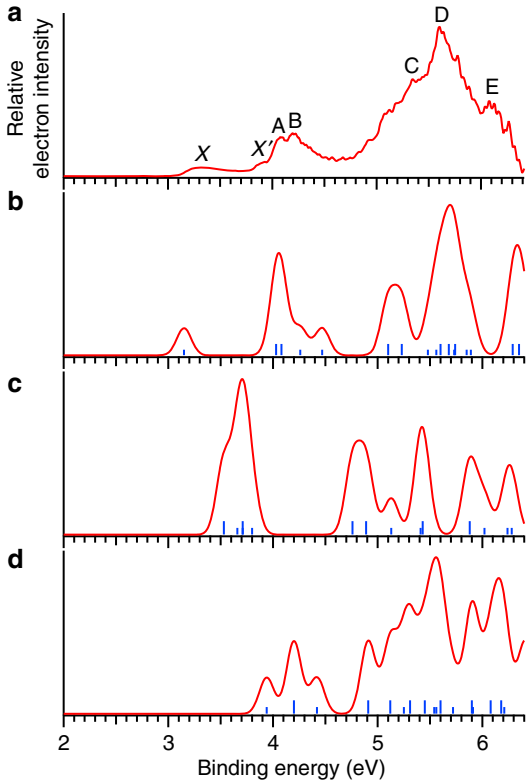

Figure 1 | Photoelectron spectroscopy of B_{36}^- and comparison with simulation. (**a**) The experimental spectrum at 193 nm. (**b**) The simulated spectrum for the global minimum quasiplanar structure with a hexagonal hole (I in Fig. 2a). (**c**) The simulated spectrum for the tubular isomer (II in Fig. 2a). (**d**) The simulated spectrum for the quasiplanar structure with two holes (III in Fig. 2a). The vertical bars in the simulated spectra represent the calculated VDEs. The simulated spectra were obtained by fitting the VDEs with a unit area Gaussian function of 0.05 eV width.

Computational results. We searched for energetically low-lying isomers of B_{36}^- with the Cartesian Walking (CW) method[19] and TGmin[24], a constrained Basin–Hopping code using energies from density functional theory (DFT). Among the 3,000 or so trial structures in our search, a quasiplanar pseudo-C_{6v} structure with a hexagonal hole was found to be much more stable than any other isomers. We also considered a ring-type structure, which was shown to be stable for large boron clusters[13,15,20,25–27]. Refined geometry optimizations and vibrational frequency calculations were performed using DFT method with the hybrid PBE0[28] exchange-correlation functional with the 6-311G* basis

set[29] on all structures within 70 kcal mol^{-1} of the pseudo-C_{6v} global minimum structure (Supplementary Fig. 1). Zero-point energy corrections were included for all the isomers at the PBE0/6-311G* level. The effect of including the zero-point corrections was small for isomers of similar structures but could be substantial (shifting relative energy values by around 2 kcal mol^{-1}) for isomers of different structural types (that is, 2D versus 3D). We found that the hexagonal global minimum structure of B_{36}^- and its corresponding neutral species exhibit C_{2v} (pseudo-C_{6v}) and C_{6v} symmetries, respectively (Fig. 2). The nearest isomers of B_{36}^-, a triple ring and a double-hole quasiplanar structure, lie 10.5 and 14.7 kcal mol^{-1} higher in energy at the PBE0 level of theory. Our global search also led to a number of other 3D structures, such as cage-like structures and two-layer structures, which are all much higher in energy (see Supplementary Fig. 1). Cartesian coordinates of the three lowest-lying structures of B_{36}^- and B_{36} (Fig. 2) are given in Supplementary Table 2.

Comparison of experimental and simulated spectra of B_{36}^-. To confirm the global minimum of B_{36}^-, we compare its simulated spectrum with the experimental data in Fig. 1 and Supplementary Table 1. The relatively simple spectral pattern can act as an electronic fingerprint. The overall simulated spectral pattern of the C_{2v} global minimum of B_{36}^- (Fig. 1b) is in good accord with the experimental spectrum. In particular, the calculated first and second VDEs are in excellent agreement with the experimental observation, confirming the large HOMO–LUMO gap observed and the unusually low EA of B_{36}. The LUMO of the hexagonal B_{36} (C_{6v}) is doubly degenerate with e_2 symmetry (Supplementary Fig. 2). The C_{2v} symmetry of B_{36}^- is, hence, due to the Jahn–Teller effect as a result of the occupation of the degenerate LUMO in the anion. The broad X band is consistent with a significant geometry change between the anionic and neutral B_{36}, primarily involving the distortion of the hexagonal hole in the anion (Supplementary Fig. 3).

However, the higher binding energy side of the experimental spectrum (Fig. 1a) is complicated and is not reproduced well by the simulated spectrum of the C_{2v} global minimum of B_{36}^- (Fig. 2b). Furthermore, the weak peak labelled as X′ observed experimentally was not reproduced by the simulated spectrum of the C_{2v} B_{36}^-, consistent with the suggestion that it might be due to a low-lying isomer. We further tested the possibility of isomer contributions by computing the VDEs for the two lowest-lying isomers (II and III in Fig. 2a), as presented in Fig. 1c,d and Supplementary Tables 3 and 4, respectively. The first five detachment channels of the tubular isomer II are close to each other around 3.7 eV (Fig. 1c and Supplementary Table 3), corresponding to the gap region between bands X and A. Thus, isomer II can be ruled out as a discernible contributor to the observed spectrum. On the other hand, the first detachment channel of isomer III is in good agreement with the X′ band (Fig. 1d and Supplementary Table 4). Furthermore, the second and third detachment channels of isomer III agree well with the broad band B, and the higher detachment channels of isomer III also seem to coincide with the congested higher binding energy part of the experimental spectrum. However, isomer III is 14.7 kcal mol^{-1} higher than the global minimum isomer I at the PBE0 level and it is not expected to be populated in any significant amount because our cluster beam is expected to be fairly cold. Under similar experimental conditions, van der Waals complexes of Ar and anionic gold clusters were observed,[30] indicating a vibrational temperature of <200 K. We then calculated the energies of the first three isomers using the more accurate, but computationally more demanding, CCSD level[31] of theory with the 6-31 + G* basis set[32] (Fig. 2a) and found that the double hole quasiplanar isomer III became more stable, only 1.17 kcal mol^{-1} above the global minimum C_{2v} isomer. Thus, isomer III would be expected to be substantially populated experimentally. The tubular isomer became 23.97 kcal mol^{-1} above the global minimum and its presence in our experiment can be safely ruled out. The combination of the simulated spectra of isomers I and III and their close energetic stability provide a much satisfying agreement with the experimental observations, lending considerable credence for the identified C_{2v} global minimum with a hexagonal hole for B_{36}^-.

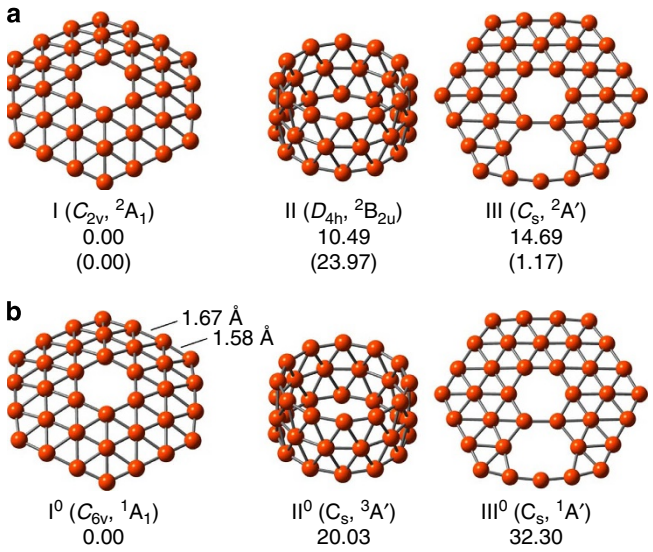

Figure 2 | The global minimum and low-lying isomers of B_{36}^- and B_{36}. (**a**) Relative energies for the isomers of B_{36}^- are given in kcal mol^{-1} at the PBE0/6-311G* and CCSD/6-31 + G*//PBE0/6-311G* (in parenthesis) levels of theory. (**b**) Relative energies for the isomers of B_{36} are given in kcal mol^{-1} at the PBE0/6-311G* level of theory. All energies have been corrected for zero-point energies at the PBE0/6-311G* level.

The electronic structure and stability of the hexagonal B_{36}. Our calculations show that neutral B_{36} has perfect hexagonal symmetry (C_{6v}) and is overwhelmingly stable relative to the closest-lying isomers II or III (Fig. 2b). The hexagonal B_{36} has an out-of-plane distortion with the shape of a bowl, and its valence molecular orbitals are shown to be similar to those of a planar structure optimized with D_{6h} constraint. DFT calculations at the PBE0/6-311G* level of theory show that the D_{6h} structure is a saddle point at $\sim$9 kcal mol^{-1} above the C_{6v} global minimum. The peripheral B–B bonding is enhanced upon shortening the B–B distance, which induces the out-of-plane bending in B_{36} to the C_{6v} bowl shape. The bowl height is 1.16 Å with two different types of peripheral B–B distances, which are reduced from 1.61 and 1.72 Å in D_{6h} to 1.58 and 1.67 Å, respectively, in the C_{6v} structure (I^0 in Fig. 2b). The shorter bond length occurs between the six apex B atoms and their neighbours (1.58 Å), while the remaining six peripheral B–B bonds are slightly longer (1.67 Å). We analysed the chemical bonding of the hexagonal C_{6v} B_{36} as well as the D_{6h} form of the cluster using adaptive natural density partitioning (AdNDP)[33], which localizes the computed density matrix into *n*-centre two-electron (*n*c-2e) bonds, with *n* ranging from one to the total number of atoms in the molecule. The AdNDP analysis of the D_{6h} structure is shown in Fig. 3; an analysis of the C_{6v} structure leads to similar results. AdNDP reveals 12 2c-2e σ bonds describing the shorter B–B bonds involving the six apex B atoms, 12 3c-2e σ bonds, 18 4c-2e σ bonds, six 4c-2e π bonds and

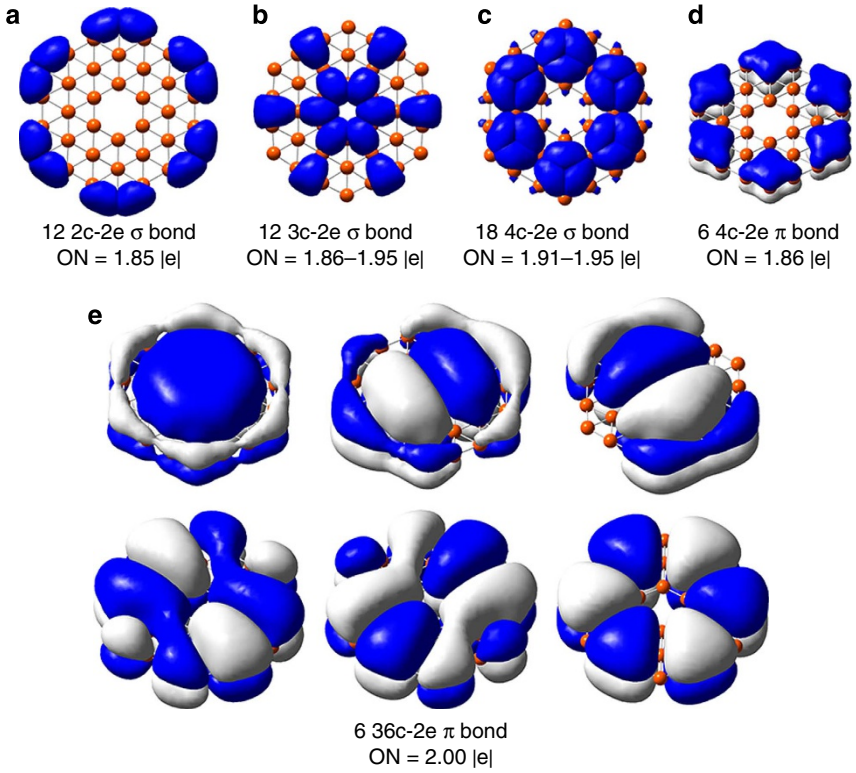

Figure 3 | Chemical bonding analysis for the hexagonal C_{6v} structure of B_{36}. The analysis was performed using the AdNDP method[33]. ON stands for occupation number and is equal to 2.00 |e| (meaning a density of exactly two electrons) in the ideal case.

six completely delocalized 36c-2e π bonds. The bonding pattern suggests that the B_{36} cluster can be viewed as six hexagonal B_7 ($B©B_6$) units bound together by the 12 3c-2e σ bonds and the six 36c-2e π bonds. The totally delocalized 36c-2e π bonds in B_{36} are interesting, which may be partly responsible for the remarkable stability of this hexagonal boron cluster.

The necessity of hexagonal holes in stable planar 2D boron sheets was analysed in detail by Tang and Ismail-Beigi[8], who considered the electronic structures of a graphene-like hexagonal boron sheet and a triangular boron lattice. They also showed a model B_{32} cluster with a hexagonal hole to be more stable than a double ring structure. To explore the effect of the hexagonal hole on the stability of the B_{36} cluster, we also optimized the structure of a B_{37} cluster with C_{6v} symmetry by filling the hexagonal hole in B_{36} with an extra B atom. We found that this B_{37} cluster with a triangular lattice has an open-shell quartet electronic state with a (a_1) (ref. 1) (e_2) (ref. 2) configuration. The optimized structure is found to have changed significantly from the C_{6v} B_{36} cluster: buckling of certain boron atoms was observed in contrast to the smooth bowl shape in the parent B_{36}. This buckling of the B_{37} cluster is similar to the buckled 2D boron sheets with triangular lattices[4–8]. The calculated atomization energy per B atom at the PBE/TZ2P level[34,35] reduces from 130.8 kcal mol^{-1} (5.67 eV per atom) for the C_{6v} B_{36} cluster to 128.9 kcal mol^{-1} (5.59 eV per atom) for the C_{6v} B_{37} cluster. Interestingly, the difference in the atomization energy (~0.08 eV per atom) between the hexagonal C_{6v} B_{36} and the buckled B_{37} cluster is also similar to that of the most stable 2D boron sheet with hexagonal holes and the buckled triangular 2D sheet (~0.11 eV per atom) at the DFT GGA level[8].

The relationship of the hexagonal B_{36} and 2D boron sheets. The hexagonal hole in the B_{36} cluster is reminiscent of the hexagonal vacancies in the 2D boron sheets recently predicted[8,9].

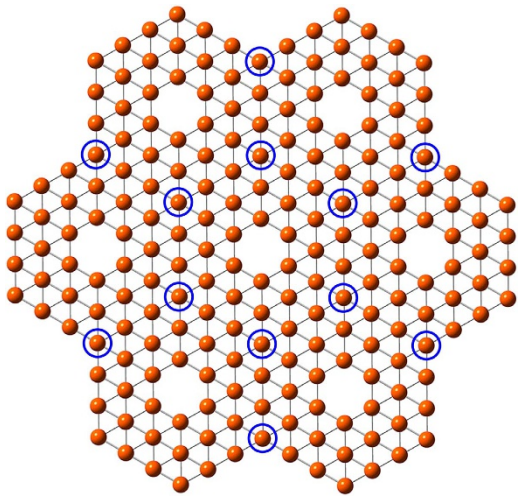

Figure 4 | Relationship between B_{36} and borophene. A schematic view of part of an extended one-atom-thick boron sheet, named borophene, as constructed from the planar hexagonal B_{36} unit. The circles represent the apex atoms in the B_{36} unit that are shared by three units. Removal of these atoms would lead to the α-sheet[8].

The B_{36} cluster can be viewed as the analogous boron unit of the hexagonal C_6 unit in graphene to form extended graphene-like boron nanostructures with hexagonal holes, as shown schematically in Fig. 4. The structure shown in Fig. 4 represents a hexagonal hole density of $\eta = 1/27$ (one vacancy per 27 lattice sites in a triangular lattice), as defined for the 2D boron sheet[8]. The structure in Fig. 4 is constructed by sharing a row of B atoms between two neighbouring B_{36} units. The apex atoms (circled in Fig. 4) are shared by three neighbouring B_{36} units. If these atoms

are removed, one arrives at the more stable α-sheet with $\eta = 1/9$ (refs 8,9). Interestingly, a B_{30} model has been used to analyse the bonding in the proposed α-sheet[36], which is equivalent to removing all six apex B atoms in the B_{36} cluster. Hence, the B_{36} cluster can be viewed as the embryo for the various proposed stable 2D boron sheets.

However, it should be pointed out that Fig. 4 is only schematically showing the relationship between the hexagonal B_{36} cluster and the stable 2D boron sheet. It does not represent the growth mechanism of the putative boron sheet, as it has been shown computationally that large boron clusters exhibit polymorphism with close-lying 3D cage-like structures[37,38]. Liu *et al.*[39] have considered computationally possible synthesis of 2D boron sheets on coinage metal surfaces as substrates, analogous to the synthesis of graphene. Thus, B_{36} or other small boron clusters with hexagonal holes may serve as the nuclei for the formation of large-scale 2D boron sheets on the substrate.

Discussion

The present study provides the first experimental evidence for the viability of novel boron nanostructures with hexagonal vacancies. These structures can indeed exist and may be synthesized using appropriate substrates[39]. The potential large-scale synthesis of the new atom-thick boron nanosheets calls for an appropriate name: 'borophene' is proposed here, in analogy to graphene. The electronic structure of the 2D boron sheets can be either metallic or semiconducting, according to theoretical calculations[8,9,22,23]. Owing to the hexagonal holes, various chemical modifications are possible to tune the electronic and chemical properties of borophenes[40,41]. Thus, borophene may constitute a new class of atom-thick nanostructures complementary to graphene.

Methods

Photoelectron spectroscopy. The experiment was performed using a PES apparatus equipped with a magnetic-bottle photoelectron analyser and a supersonic cluster source[42]. Boron cluster anions (B_x^-) were produced by laser vaporization of a hot-pressed boron target made of ^{10}B-enriched powder with a helium carrier gas seeded with 5% argon, which was shown previously to produce cold clusters[30]. The clusters were entrained in the carrier gas and underwent a supersonic expansion. Negatively charged clusters were extracted from the cluster beam and analysed by a time-of-flight mass spectrometer. Clusters of interest were mass-selected, decelerated and photodetached by a laser beam at 266 and 193 nm. The photoelectron spectra were measured using a magnetic-bottle PES analyser and calibrated by the known spectra of Au^- and Bi^-. The resolution (ΔEk/Ek) of the magnetic-bottle analyser was 2.5%—that is, 25 meV for 1 eV electrons.

Computational and theoretical methods. DFT global minimum searches were carried out using two methods, the CW method and a constrained Basin–Hopping method in the TGMin code[24]. The CW method has been described in detail elsewhere[19]. The CW search of B_{36}^- used DFT for energy evaluation, employing the PBE functional and the 3-21G basis set[43] from the Gaussian 09 program[44]. Within roughly 500 trial structures, a quasiplanar structure of near C_{6v} symmetry with a central hexagonal hole was found to be low in energy. We re-optimized all trial structures under 20 kcal mol^{-1} at the PBE0/3-21G level; the pseudo-C_{6v} structure remained the lowest in energy.

Using the TGMin code we performed a more thorough search for the global minimum of B_{36}^-. The calculations were carried out using the DFT formalism with the PBE exchange-correlation functional and the Goedecker–Teter–Hutter pseudopotential[45] with the associated double-ζ valence plus polarization basis set[35] for boron via the CP2K program[46]. Among more than 2,500 possible structures produced by TGMin and the manually built tubular structures, we located a bowl-shaped pseudo-C_{6v} isomer with a hexagonal hole in the centre as the global minimum of B_{36}^- (Fig. 1a), in agreement with the CW result. Further analyses and geometry optimizations indicate that the actual symmetries of this anion and its neutral cluster are C_{2v} and C_{6v}, respectively. We further refined the energies by reoptimizing the geometries of low-lying isomers within 70 kcal mol^{-1} of the global minimum using DFT method with the hybrid PBE0 functional and the 6-311G* basis set from the Gaussian 09 program. Vibrational frequencies were calculated for each isomer and all the structures were ensured to be minima on the potential energy surface without imaginary frequencies. The re-optimized geometric structures and the PBE0 energies of the low-lying structures within 63 kcal mol^{-1} of the global minimum are given in Supplementary Fig. 1. For more accurate relative energy assessment, single point calculations for the three lowest lying isomers were carried out using the CCSD formalism with the 6-31 + G* basis set at their corresponding PBE0/6-311G* geometries using the Molpro software package[47–49].

We calculated the VDEs for the three low-lying structures to compare with the experimental photoelectron spectrum. The VDEs were computed using an approach named ΔSCF-TDDFT previously[50,51]. In this approach, the ground-state energies of the anions and the neutrals were calculated at the optimized geometries of the anions from the ΔSCF energy differences at the PBE0/6-311 + G* level of theory, whereas the vertical excited-state energies of the electron-detached neutral species were obtained from TDDFT calculations at the geometries of the anions. These excitation energies were then added to the first VDE to approximate the high-lying VDEs. Only those neutral excited states with one-electron detachment from the anion ground state were chosen. The relative intensities used for the VDEs were assigned empirically on the basis of the spin multiplicities of the final states, one for singlet and two for triplet final states. The simulated PES spectra were constructed by fitting the distribution of the VDEs with unit-area Gaussian functions of 0.07 eV full width at half-maximum. This approach has been used extensively in elucidating the structures of size-selected clusters previously[16–21].

References

1. Iijima, S. Helical microtubules of graphitic carbon. *Nature* **354,** 56–58 (1991).
2. Boustani, I. & Quandt, A. Nanotubules of bare boron clusters: *ab initio* and density functional study. *Europhys. Lett.* **39,** 527–532 (1997).
3. Gindulyté, A., Lipscomb, W. & Massa, N. L. Proposed boron nanotubes. *Inorg. Chem.* **37,** 6544–6545 (1998).
4. Boustani, I., Quandt, A., Hernandez, E. & Rubio, A. New boron based nanostructure materials. *J. Chem. Phys.* **110,** 3176–3185 (1999).
5. Evans, M. H., Joannopoulos, J. D. & Pantelides, S. T. Electronic and mechanical properties of planar and tubular boron structures. *Phys. Rev. B* **72,** 045434 (2005).
6. Kunstmass, J. & Quandt, A. Broad boron sheets and boron nanotubes: an ab initio study of structural, electronic, and mechanical properties. *Phys. Rev. B* **74,** 035413 (2006).
7. Lau, K. C. & Pandey, R. Stability and electronic properties of atomistically-engineered 2D boron sheets. *J. Phys. Chem. C* **111,** 2906–2912 (2007).
8. Tang, H. & Ismail-Beigi, S. Novel precursors for boron nanotubes: the competition of two-center and three-center bonding in boron sheets. *Phys. Rev. Lett.* **99,** 115501 (2007).
9. Yang, X., Ding, Y. & Ni, J. Ab initio prediction of stable boron sheets and boron nanotubes: structure, stability, and electronic properties. *Phys. Rev. B* **77,** 041402 (2008).
10. Szwacki, N. G., Sadrzadeh, A. & Yakobson, B. I. B_{80} fullerene: an *ab initio* prediction of geometry, stability, and electronic structure. *Phys. Rev. Lett.* **98,** 166804 (2007).
11. Zhai, H. J., Alexandrova, A. N., Birch, K. A., Boldyrev, A. I. & Wang, L. S. Hepta- and octacoordinate boron in molecular wheels of eight- and nine-atom boton clusters: observation and confirmation. *Angew. Chem. Int. Ed.* **42,** 6004–6008 (2003).
12. Zhai, H. J., Kiran, B., Li, J. & Wang, L. S. Hydrocarbon analogues of boron clusters – planarity, aromaticity and antiaromaticity. *Nat. Mater.* **2,** 827–833 (2003).
13. Kiran, B. *et al.* Planar-to-tubular structural transition in boron clusters: B_{20} as the embryo of single-walled boron nanotubes. *Proc. Natl Acad. Sci. USA* **102,** 961–964 (2005).
14. Alexandrova, A. N., Boldyrev, A. I., Zhai, H. J. & Wang, L. S. All-boron aromatic clusters as potential new inorganic ligands and building blocks in chemistry. *Coord. Chem. Rev.* **250,** 2811–2866 (2006).
15. Oger, E. *et al.* Boron cluster cations: transition from planar to cylindrical structures. *Angew. Chem. Int. Ed.* **46,** 8503–8506 (2007).
16. Sergeeva, A. P., Zubarev, D. Y., Zhai, H. J., Boldyrev, A. I. & Wang, L. S. A photoelectron spectroscopic and theoretical study of B_{16}^- and B_{16}^{2-}: an all-boron naphthalene. *J. Am. Chem. Soc.* **130,** 7244–7246 (2008).
17. Sergeeva, A. P., Averkiev, B. B., Zhai, H. J., Boldyrev, A. I. & Wang, L. S. All-boron analogues of aromatic hydrocarbons: B_{17}^- and B_{18}^-. *J. Chem. Phys.* **134,** 224304 (2011).
18. Huang, W. *et al.* A concentric planar doubly π-aromatic B_{19}^- cluster. *Nat. Chem.* **2,** 202–206 (2010).
19. Piazza, Z. A. *et al.* A photoelectron spectroscopy and *ab initio* study of B_{21}^-: negatively charged boron clusters continue to be planar at 21. *J. Chem. Phys.* **136,** 104310 (2012).
20. Sergeeva, A. P. *et al.* B_{22}^- and B_{23}^-: all-boron analogues of anthracene and phenanthrene. *J. Am. Chem. Soc.* **134,** 18065–18073 (2012).
21. Popov, I. A., Piazza, Z. A., Li, W. L., Wang, L. S. & Boldyrev, A. I. A combined photoelectron spectroscopy and *ab initio* study of the quasi-planar B_{24}^- cluster. *J. Chem. Phys.* **139,** 144307 (2013).
22. Penev, E. S., Bhowmick, S., Sadrzadeh, A. & Yakobson, B. I. Polymorphism of two-dimensional boron. *Nano Lett.* **12,** 24412445 (2012).

23. Wu, X. *et al.* Two-dimensional boron monolayer sheets. *ACS Nano* **6,** 7443–7453 (2012).
24. Zhao, Y. F. & Li, J. TGMin: a global minimum search code based on basin-hopping and divide-and-concur strategy. *Nano Res* (in press).
25. An, W., Bulusu, S., Gao, Y. & Zeng, X. C. Relative stability of planar versus double-ring tubular isomers of neutral and anionic boron cluster B_{20} and B_{20}^-. *J. Chem. Phys.* **124,** 154310 (2006).
26. Tian, F. Y. & Wang, Y. X. The competition of double-, four-, and three-ring tubular B_{3n} ($n=8$–32) nanoclusters. *J. Chem. Phys.* **129,** 024903 (2008).
27. Tai, T. B., Tam, N. M. & Nguyen, M. T. Structure of boron clusters revisited, B_n with $n=14$–20. *Chem. Phys. Lett.* **530,** 71–76 (2012).
28. Adamo, C. & Barone, V. Toward reliable density functional methods without adjustable parameters: the PBE0 model. *J. Chem. Phys.* **110,** 6158–6165 (1999).
29. Krishnan, R., Binkley, J. S., Seeger, R. & Pople, J. A. Self-consistent molecular orbital methods. XX. A basis set for correlated wave functions. *J. Chem. Phys.* **72,** 650–654 (1980).
30. Huang, W. & Wang, L. S. Probing the 2D-to-3D structural transition in gold cluster anions using argon-tagging. *Phys. Rev. Lett.* **102,** 153401 (2009).
31. Cizek, J. On the use of the cluster expansion and the technique of diagrams in calculations of correlation effects in atoms and molecules. *Adv. Chem. Phys.* **14,** 35–89 (1969).
32. Francl, M. M. *et al.* Self-consistent molecular orbital methods. XXIII. A polarization-type basis set for second-row elements. *J. Chem. Phys.* **77,** 3654–3665 (1982).
33. Zubarev, D. Y. & Boldyrev, A. I. Developing paradigms of chemical bonding: adaptive natural density partitioning. *Phys. Chem. Chem. Phys.* **10,** 5207–5217 (2008).
34. Perdew, J. P., Burke, K. & Ernzerhof, M. Generalized gradient approximation made simple. *Phys. Rev. Lett.* **77,** 3865–3868 (1996).
35. Vandevondele, J. & Hutter, J. Gaussian basis sets for accurate calculations on molecular systems in gas and condensed phases. *J. Chem. Phys.* **127,** 114105 (2007).
36. Galeev, T. R. *et al.* Deciphering the mystery of hexagonal holes in an all-boron graphene α-sheet. *Phys. Chem. Chem. Phys.* **13,** 11575–11578 (2011).
37. Prasad, D. L. V. K. & Jemmis, E. D. Stuffing improves the stability of fullerenelike boron clusters. *Phys. Rev. Lett.* **100,** 165504 (2008).
38. De, S. *et al.* Energy landscape of fullerene materials: a comparison of boron to boron nitride and carbon. *Phys. Rev. Lett.* **106,** 225502 (2011).
39. Liu, Y., Penev, E. S. & Yakobson, B. I. Probing the synthesis of two-dimensional boron by first-principles computations. *Angew. Chem. Int. Ed.* **52,** 3156–3159 (2013).
40. Tang, H. & Ismail-Beigi, S. Self-doping in boron sheets from first principles: a route to structural design of metal boride nanostructures. *Phys. Rev. B* **80,** 134113 (2009).
41. Er, S., de Wijs, G. A. & Brocks, G. DFT study of planar boron sheets: a new template for hydrogen storage. *J. Phys. Chem. C* **113,** 18962–18967 (2009).
42. Wang, L. S., Cheng, H. S. & Fan, J. W. Photoelectron spectroscopy of size-selected transition metal clusters: Fe_n^-, $n=3$–24. *J. Chem. Phys.* **102,** 9480–9493 (1995).
43. Binkley, J. S., Pople, J. A. & Hehre, W. J. Self-consistent molecular orbital methods. 22. Small split-valence basis sets for second-row elements. *J. Am. Chem. Soc.* **104,** 2797–2803 (1982).
44. Frisch, M. J. *et al. Gaussian 09, Revision A.1* (Gaussian Inc., 2009).
45. Goedecker, S., Teter, M. & Hutter, J. Separable dual-space gaussian pseudopotentials. *Phys. Rev. B* **54,** 1703–1710 (1996).
46. Vandevondele, J. *et al.* QUICKSTEP: fast and accurate density functional calculations using a mixed gaussian and plane waves approach. *Comput. Phys. Commun.* **167,** 103–128 (2005).
47. Werner, H.-J., Knowles, P. J., Knizia, G., Manby, F. R. & Shutz, M. Molpro: a general-purpose quantum chemistry program package. *WIREs Comput. Mol. Sci.* **2,** 245–253 (2012).
48. Hampel, C., Peterson, K. & Werner, H.-J. A comparison of the efficiency and accuracy of the quadratic configuration interaction (QCISD), coupled cluster (CCSD), and Brueckner coupled cluster (CSSD) method. *Chem. Phys. Lett* **190,** 1–12 (1992).
49. Werner, H.-J. *et al.* MOLPRO, version 2012.1, a packge of *ab initio* programs. See http://www/molpro.net.
50. Li, X., Kiran, B., Li, J., Zhai, H. J. & Wang, L. S. Experimental observation and confirmation of icosahedral $W@Au_{12}$ and $Mo@Au_{12}$ molecules. *Angew. Chem. Int. Ed.* **41,** 4786–4789 (2002).
51. Li, J., Li, X., Zhai, H. J. & Wang, L. S. Au_{20}: a tetrahedral cluster. *Science* **299,** 864–867 (2003).

Acknowledgements

We thank Dr C. Romanescu and Dr H. J. Zhai for earlier experimental assistance. We are indebted to Professor A. I. Boldyrev for discussions and assistance in the development of the Cartesian Walk method and to Dr Dezhi Wang (Boston College) for help in preparing the hot-pressed boron target. The experimental work was supported by the National Science Foundation (CHE-1263745). This work used the Extreme Science and Engineering Discover Environment (XSEDE), which was supported by the National Science Foundation (OCI-1053575). The theoretical work performed at the Tsinghua University was supported by NKBRSF (2011CB932400) and NSFC (20933003, 91026003) of China. The calculations were performed using the Center for Computation and Visualization (CCV) at Brown University, the Supercomputer Center of the Computer Network Information Center at the Chinese Academy of Sciences and the Molecular Science Computing capability at the EMSL, a national scientific user facility sponsored by the Department of Energy's Office of Biological and Environmental Research and located at PNNL, a multiprogram national laboratory operated for the Department of Energy by Battelle.

Author contributions

W.-L.L performed the experiment and analysed the data. Z.A.P., H.-S.H. and Y.-F.Z. did the calculations. L.-S.W. and J.L. designed the research. Z.A.P., W.-L.L., J.L. and L.-S.W. co-wrote the paper.

Additional information

Supplementary Information accompanies this paper at http://www.nature.com/naturecommunications

Competing financial interests: The authors declare no competing financial interests.

Reprints and permission information is available online at http://npg.nature.com/reprintsandpermissions/

How to cite this article: Piazza, Z. A. *et al.* Planar hexagonal B_{36} as a potential basis for extended single-atom layer boron sheets . *Nat. Commun.* 5:3113 doi: 10.1038/ncomms4113 (2014).